TEPES
TURKISH JOURNAL OF
ELECTRICAL POWER
AND ENERGY SYSTEMS

TEPES, Vol. 4, Issue. 1, 13-25, 2024 **DOI:** 10.5152/tepes.2024.23026

RESEARCH ARTICLE

Coordination of Flexible Alternating Current Transmission Systems and Distributed Generation in a Synthetic Co-simulation of Transmission and Distribution Network

Ahmad Abubakar Sadiq[1], Latifa Yusuf[2], Muhammad Buhari[3], Sunusi Sani Adamu[3], James Garba Ambafi[1]

[1]Department of Electrical and Electronic Engineering, Federal University of Technology, Minna, Nigeria
[2]University of Victoria, British Columbia, Canada
[3]Department of Electrical Engineering, Bayero University Kano, Nigeria

Cite this article as: A. A. Sadiq, L. Yusuf, M. Buhari, S. Sani Adamu and J. Garba Ambafi, "Coordination of flexible alternating current transmission systems and distributed generation in a synthetic co-simulation of transmission and distribution network," *Turk J Electr Power Energy Syst.*, 2024; 4(1), 13-25.

ABSTRACT

In ensuring sustainable power delivery under rapid growth in demand, modern power grids are characterized by advanced solutions such as flexible alternating current transmission systems and distributed generation. However, flexible alternating current transmission systems and distributed generations are often planned by their respective system operators, ignoring their coordination and impacting system-wide performance. This paper develops a bi-level optimization approach for flexible alternating current transmission systems and distributed generation coordination in an integrated transmission and distribution network to improve available transfer capability, power losses, and voltage deviation. The approach comprises inner and outer optimization. Inner optimization implements a hybrid of particle swarm optimization and Active Power Flow Performance Index for flexible alternating current transmission systems' planning. At the same time, the outer optimization employs multi-objective particle swarm optimization, which targets distributed generation planning at the distribution network—the integrated transmission and distribution network models' both transmission and distribution section. To demonstrate the effectiveness of the developed approach, two models of distributed generations, only real power and real and reactive power injections, were separately coordinated with a thyristor-controlled series compensator and static synchronous series compensator. Results show superior available transfer capability enhancement with thyristor-controlled series compensator–power injections$_{DG}$ and static synchronous series compensator–power injections$_{DG}$, compared to the non-coordinated scenario. Pareto front plots of available transfer capability, power losses, and voltage deviation are such that after some maximum available transfer capability, the slope of the Pareto approaches zero.

Index Terms—Coordination, distributed generation, FACTS, integrated transmission and distribution network, particle swarm optimization

I. INTRODUCTION

In the modern transmission grid, flexible alternating current transmission systems (FACTS) devices are deployed for sustainable power delivery by improving power flows, transfer capability, damping oscillations, and ensuring flexible operations and control [1-3]. In contrast, modern distribution networks (DN) are required to accommodate large penetration of distributed generation (DG) [4-6], which seldom has adequate reactive support. Maintaining power flows and voltages within limits due to increased DG penetration [7] requires coordination and reactive compensation from FACTS [8]. Furthermore, the penetration of DG into the DN and the emergence of active DN, driven primarily by the decarbonization of the power supply chain [9], has brought about new challenges in the power system's planning and operations as a single entity [10]. Among the challenges of active DNs to system operators is the inadequate understanding of the interactions between DGs and the installed compensating devices at the transmission section, such as FACTS [11] or synchrophasor units for multi-area state estimation [12]. Also, the benefits provided by FACTS devices to the entire power grid not only depend on optimal location and sizing but also on their coordination with other components providing similar services at the distribution voltage level. The power DN is a critical part of the power grid, and failure of its associated components, like DG, may cause local outages and ripple effects with system-wide impacts [13].

Received: November 26, 2023
Revision Requested: December 11, 2023
Last Revision Received: December 22, 2023
Accepted: January 12, 2024
Publication Date: February 15, 2024

Corresponding author: Ahmad Abubakar Sadiq, ahmad.abubakar@futminna.edu.ng

Although FACTS and DGs are common features of the modern power grid, they are often treated as separate entities in planning studies. This is because FACTS and DGs are often managed at transmission and distribution voltage levels, respectively, belonging to different systems operators and without adequate coordination of their impacts [14]. The high voltage section with or without FACTS is assumed to be stable in DG planning. It ignores the impacts of FACTS control operation. Similarly, FACTS planning assumes a passive DN as a lumped constant power load [9]. Both assumptions either ignore the system-wide impacts of FACTS' control or the involvement of DG in the emergence of an active DN and ancillary service provision [15]. For a given network, the increased power demand in the presence of uncoordinated FACTS and DG planning causes poor power system performance [16].

Consequently, the size and complex nature of the grid, the system operators' prerogatives, and the need for reliable operation of power systems as a single entity, hitherto planned separately [17], constitute the challenges in planning, operations, and coordination of power grid's components as a single entity [18]. Owing to the rising penetration of DG and deployment of FACTS devices, the conventional planning and operating approaches that distinguish the transmission and distribution system are no longer efficient [19], resulting in suboptimal solutions [20]. Accordingly, this paper develops a bi-level optimization approach for FACTS and DG coordination in a co-simulated transmission and DN called an integrated transmission and DN (iT & DN).

Main Points

- The study develops a generalized bi-level optimization for coordinated planning of flexible alternating current transmission systems (FACTS) and distributed generation (DG): the coordination includes FACTS devices with single and multiple control variables, such as thyristor-controlled series compensator (TCSC) and static synchronous series compensator (SSSC). The contribution in this paper focuses on SSSC's voltage injection measured by the voltage vector V_{se} and δ_{se}. This constitutes two control variables, unlike the TCSC, which has a single variable.
- The study models and deploys an integrated test network comprising both transmission and distribution sections to demonstrate generalized FACTS and DG coordination: the synthetic network provides the semblance of a real-world power systems network as a single entity, thereby allowing the simulation of both transmission and distribution network resources such as SSSC and DG, respectively.
- The study demonstrates the coordination of TCSC and SSSC with real power and reactive power DG models: FACTS coordination with different DG models simulates the features of some renewable energy DGs with or without reactive power support.
- The study establishes the correlation between objectives (available transfer capability, power loss, voltage deviations) through three-dimensional Pareto front: the correlation among the objectives provides essential information on the size limit of FACTS since larger sizes may not translate to improved benefits.

II. RELATED WORKS

The coordination of multiple FACTS devices, such as the thyristor-controlled series compensator (TCSC), static var compensator (SVC), and unified power flow controller (UPFC) with onload tap changer (OLTC) and generator reactive power, was presented in [21]. Similar works in [22, 23] implemented the coordination of multi-type FACTS devices for available transfer capability (ATC). However, the coordination is demonstrated at the transmission level and ignores power generation from DG units at DNs to meet increased load demand.

Consequently, to account for DGs, [24] develops an extended non-dominant sorted genetic algorithm (*E_NSGAII*) for the planning of DN in the presence of DG and distribution static compensator (DSTATCOM). However, E_NSGA II ignores the interactions between DGs and DSTATCOM on multi-objectives and considers only the DN. Similarly, the use of FACTS for stability improvement of microgrids was presented in [25] and concluded that the stability issues caused by DG can be mitigated using FACTS. Additionally, [26] demonstrated that TCSC can increase the failure margin, decrease bus voltage sensitivity to Var, and improve voltage stability. Similarly, [27] developed a method to minimize counteraction and coordinate SVC and OLTC in the presence of DG-induced disturbances. The deployment of STATCOM for power quality improvement of a wind conversion system is presented in [28]; likewise, [29] discussed power quality evaluation of DG systems. However, [24–29] ignores ATC as an objective, a critical decision parameter in the deregulation framework of power transactions.

Subsequently, ATC enhancement with SVC, TCSC, and DG was demonstrated in IEEE 24 bus by [30] but ignored VAR management in FACTS and DG coordination. A strategy for planning multiple DG and SVC is presented in [31]. Results show increased power losses with DG without VAR coordination. Also, [32] presented coordination between DG and DSTATCOM for reactive power management; again, it is limited to the DN and ignores FACTS' control operations. Similarly, simultaneous reconfiguration and planning of DSTATCOM and DG in a distribution system are reported in [33]. The formulation involves multi-objective, and again, the study ignores the interaction between DG and DSTATCOM and is limited to DN.

Although in [8], [21–27], some consider FACTS and DGs planning simultaneously, their interactions and, consequently, their coordination was not adequately considered. Furthermore, [30–33] focuses on DNs and ignores transmission-based FACTS control operations. Accordingly, the coordination of UPFC and DGs is discussed in [34]. It was observed that power transferred on the lines increases when UPFC is coordinated with DG. However, the extent of power transfer and interactions between UPFC and DG were unclear. Also, transfer capability is treated in terms of tie lines rather than system-wide effects. Furthermore, the impact assessment of DG in synchronism with SVC is discussed by [35]. In contrast, [36] discusses the integration of the wind power plant and TCSC location. It is concluded that TCSC significantly reduces the load curtailment and improves supply from wind energy sources. The test networks in [35, 36] were limited to distribution.

Therefore, FACTS and DG coordination entail distinct objectives due to the prerogatives of system operators. Thus, a multi-level optimization approach is suitable. A multi-objective framework is presented in [37] for the optimal interface of energy hubs and DN. The operation cost of DN and the cost of each energy hub are the upper and lower-level objectives. However, the multi-objectives were converted into a single objective, which de-emphasizes the correlation between objectives and energy sources.

Consequently, this paper develops a bi-level method of coordinated planning of FACTS and DG in an *iT&DN* to enhance ATC, reduce power losses (P_{loss}) and voltage deviation (V_D). These objectives were independently treated to obtain their correlation. Two series FACTS, TCSC, and static synchronous series compensator (SSSC), were coordinated with DG's models (PV and PQ). The central points of this paper are:

- Develop a generalized bi-level optimization for coordinated planning of FACTS and DG.
- Models and deploys an integrated test network comprising transmission and distribution sections to demonstrate generalized FACTS and DG coordination.
- Demonstrate the coordination of TCSC and SSSC with PV and PQ models of DG.
- Establishes the correlation between objectives (ATC, power loss, *VD*s) through three-dimensional (3D) Pareto front.

The rest of this paper is structured as follows: Section III presents the problem formulation of FACTS and DG planning with the bi-level approach, outlining the inner and outer optimization and a description of the multi-objective particle swarm optimization (MOPSO) and its sub-blocks. Section IV presents the integrated test network. Section V captures the implementation environment, which describes the integrated test network and the simulation environment. Section VI presents and discusses the results of the bi-level approach. Finally, Section VII concludes the discussed results.

III. PROBLEM FORMULATION

Optimizing the power system's performance involves multiple objectives: discrete, continuous, and belonging to distinct operators. The problem formulation often results in parallel and multi-objective optimization [9]. Also, the solution search space is prone to local optima, which various meta-heuristic approaches avoid [37–42]. Additionally, competing objectives result in an optimal solution for one objective but local for another. These prerogatives of the system operators necessitate a multi-level approach in formulating the problem, thereby providing insight into the interactions between FACTS and DG belonging to different entities.

A. The Bi-level Optimization Approach

Fig. 1 displays the graphic description for implementing the proposed bi-level optimization approach. In the coordinated planning approach of FACTS and DG, the implementation environment involves data exchange between MATLAB and MATPOWER. The approach comprises the inner and outer optimization (IO and OO) levels.

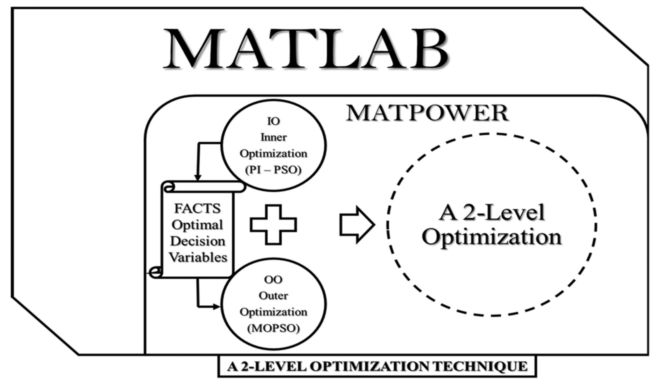

Fig. 1. Schematic of the bi-level optimization for FACTS–DG coordination. FACTS, flexible alternating current transmission systems; DG, distributed generation.

In an earlier paper [2], the IO by Hybrid Performance Index and Particle Swarm Optimization (PI–PSO) for FACTS' planning was developed. The output solutions of the PI–PSO serve as input to the OO, which implements *MOPSO* for DG planning in the DN. Coupling between inner and outer optimization levels allows for data exchange, and the problem formulation describing the coordinated scheduling of FACTS and DG is described in the following subsection.

B. Inner Optimization

Complete documentation of the inner optimization (PI–PSO) is presented in [2], such that a given particle's position is described by equation 1, where φ and η are the location (line number) and size of FACTS, respectively. In addition to position and velocity updates in the conventional PSO described in equations (2) and (3), PI–PSO imposes further strict updates to the position update as expressed in equation (4).

$$X_i^k = [\phi_i^k ; \eta_i^k] \tag{1}$$

$$X_i^{(k+1)} = X_i^k + V_i^{(k+1)} \tag{2}$$

$$V_i^{(k+1)} = \omega V_i^k + c_1 rand\left(P_{best_i}{}^k - X_i^k\right) + c_2 rand\left(G_{best_i}{}^k - X_i^k\right) \tag{3}$$

$$X_i^{(k+1)} = \begin{cases} X_i^{k+1(\phi_i)} & if\,\phi_i^{k+1} \in N \\ N(randperm(m,1) & if\ \phi_i^{k+1} \notin N \\ X_i^{k+1}(\eta_i) & for\,\eta_i \in R \end{cases} \tag{4}$$

Continuation power flow (CPF) is used to evaluate the ATC, such that the active power set points of the supply and demand bids are varied simultaneously up to the maximum loading parameter. Consequently, the ATC is to be evaluated in equation (5), which is subject to equations (6) to (12).

$$\underset{(\lambda, x_k, V_{se}, \delta_{se})}{Max}\left\{ ATC = \sum_{i \in sink} P_L^i(\lambda_{\lim}) - \sum_{i \in sink} P_L^i(\lambda_o) \right\} \tag{5}$$

Subject to:

$$f(x,\lambda)=0 \tag{6}$$

$$0\le\lambda\le\lambda_{\lim} \tag{7}$$

$$S_{ij}=S_{ij}^{rated} \tag{8}$$

$$V_i^{\min}\le V_i\le V_i^{\max} \tag{9}$$

$$Q_{\min}\le Q_g\le Q_{\max} \tag{10}$$

$$P_{\min}\le P_g\le P_{\max} \tag{11}$$

$$X_{FACTS}^{\min}\le X_{FACTS}\le X_{FACTS}^{\max} \tag{12}$$

In equation (5) P_L^i is the active power load is involved in power transfer, $\lambda_{\lim}$ and λ_0 are the loading parameters at the power transfer limit and base case, respectively. As given in equation (5), decision variables at inner optimization include active power set points of supply and demand bids modeled by loading parameter λ, TCSC reactance (x_k), and the SSSC series injected voltages modeling by $V_{se}\angle\delta_{se}$. Furthermore, equation (5) is subject to the non-linear compact power flow equation described in equation (6), where the state variable $x=(V,\ \delta)$ represents voltage magnitude and angle. The constraints equation (7) limit the loading parameter to the transfer binding constraints. Equation (8) models the thermal limit of the transmission lines in terms of the apparent power flows S_{ij}, equation (9) sets the operating voltage limits V_i^{min} and V_i^{max}, while equation (10) imposes generator reactive power Q_{min} and Q_{max}. Additionally, equations (10) and (11) describe the active and reactive power limits of the generators involved in the transactions. Limitations to FACTS's sizes are treated as constraints imposed by equation (12). The percentage compensation of TCSC is within $-0.8\le X_{Tcsc}\le 0.2$ and series injection by SSSC is ranged $0\le X_{SSSC}^{Vse}\le 0.1$. The power injection models of TCSC and SSSC were implemented as documented in [23].

C. Outer Optimization

The optimal FACTS' planning solutions are sent from the IO to the OO. Subsequently, the OO targets DG planning at the distribution section to minimize P_{loss} and V_D incurred at IO. Two objectives of OO are parallel and opposite to the ATC maximization in IO. To ensure optimal solutions at OO without deteriorating the IO solution, the approach within OO adopts an outer optimization (MOPSO). A set of non-dominated Pareto solutions comprising the three objectives of *ATC*, P_{loss}, and V_D are obtained. Decision variables at OO involve the DG locations (β_{dg}), sizes (γ_{dg}) and FACTS' size (η_{facts}) described in equation (13). The objectives at OO formulated in equation (14) are constrained by equations (6) to (12).

$$DG_{POS}=[\eta_{facts},\beta_{dg};\gamma_{dg}] \tag{13}$$

$$\underset{(\eta_{facts},\beta_{dg},\gamma_{dg})}{Min}\begin{cases}P^{loss}=\sum_{k=1}^{nl}g_k[V_i^2+V_j^2-2V_iV_j\cos\delta_{ij}]\\ V_D=\sum_{i=1}^{nb}\left|1-V_i\right|\end{cases} \tag{14}$$

Equation (1) depicts that FACTS devices have two degrees of freedom (location and size). However, in successive planning horizons, the location of an existing FACTS device is not available [21, 22]. Consequently, as expressed in equations (13) and (14), the decision variables at OO include locations and sizes of DG [β_{dg}, γ_{dg}] in coordination with FACTS' size [η_{facts}] obtained from IO. Since the objectives for *FACTS–DG* coordination involve both maximization of ATC and the minimization of P_{loss} and V_D, there is a need to transform the *MOPSO* algorithm into the same optimization front. Equation (15) describes the minimization formulation of *FACTS–DG* coordination for *m* objectives.

$$\text{minimize}\,\vec{f}(x,\lambda)=\left[f_1(x,\lambda),f_2(x,\lambda)\dots f_m(x,\lambda)\right] \tag{15}$$

Equation (15) is subject to constraints expressed in equations (6) to (12) as well as equations (16) and (17), which limit DG sizes to 75% of loads in DN [39, 43]. Where P_{load}^{dn} and Q_{load}^{dn} are the aggregate real and reactive load of DN section. Two types of DG model, depending on the ability to inject only real power, real and reactive power (PV and PQ), respectively, were coordinated with TCSC and SSSC separately [9].

$$0\le\gamma_{dg}^p\le 0.75P_{load}^{dn} \tag{16}$$

$$-0.75Q_{load}^{dn}\le\gamma_{dg}^q\le 0.75Q_{load}^{dn} \tag{17}$$

D. Fitness Evaluation in MOPSO

Equation (18) describes the complete objectives: maximization of ATC and the minimization of P_{loss} and V_D, for *FACTS–DG* coordination. In equation (18), the negated ATC transforms the entire fitness into a minimization.

$$\vec{f}(x,\lambda)=\begin{cases}-ATC=-Equation(5)\\ P^{loss}=\sum_{k=1}^{nl}g_k[(V_i^2+V_j^2)-2(V_iV_j\cos\delta_{ij})]\\ V_D=\sum_{i=1}^{nb}\left|1-V_i\right|\end{cases} \tag{18}$$

Equations (19) and (20) describe elements of the vector that model the decision variables of FACTS and DG sizes, respectively.

$$X_{facts}=\begin{cases}-jx_k;\quad -0.2\le x_k\le 0.8\\ V_{se},\delta_{se};\quad 0\le V_{se}\le 0.1,\ -\pi\le\delta_{se}\le\pi\end{cases} \tag{19}$$

$$X_{DG}=\begin{cases}\gamma_{dg}^p;\quad PV\,\text{mod}el,\quad 0\le\gamma_{dg}^p\le 0.75P_{load}^{dn}\\ \gamma_{dg}^p+\gamma_{dg}^q;\quad PQ\,\text{mod}el,\quad 0\le\gamma_{dg}^q\le 0.75Q_{load}^{dn}\end{cases} \tag{20}$$

E. Dominance Determination in MOPSO

The dominance condition of a given objective over others, $\vec{f_i}(x,\lambda)$ dominate $\vec{f_j}(x,\lambda)$, is mathematically written as $\vec{f_i}(x,\lambda)\prec\vec{f_j}(x,\lambda)$, and expressed by equation (21).

$$\begin{aligned}&\forall i\in\{1,2,3\}:f_i(x,\lambda)<f_i(x,\lambda)\,and\\ &\exists i\in\{1,2,3\}:f_i(x,\lambda)<f_i(x,\lambda)\end{aligned} \tag{21}$$

where $j = 1,2 \ldots m$ and $j \neq i$. The symbol > represents the domination concept [44]. Generally, in a non-dominated solution pair, an improvement in an objective $\vec{f}_i(x,\lambda)$ can cause the deterioration of at least one other objective. Non-dominated solutions are retained according to equation (21) in an archive [40], limited to 100 solution members, and membership is by criteria equal to the leader selection pressure.

F. Leader Selection

In conflicting objectives, a global solution is complicated; thus, a leader among non-dominated solutions is designated as a guide towards a better region in the search space. Herein, leader selection uses the Roulette wheel technique. The probability (P^i) of selecting the i_{th} particle as leader is expressed in equation (22), where P_r is as defined in equation (23), τ is the particle selection pressure, and the archive's size is N [42].

$$P^i = \frac{P_r}{\sum_{i \in N} P_r^i} \tag{22}$$

$$P^i = e^{-\tau N} \tag{23}$$

The probability of selecting particles (q_i) from the archives is expressed in equation (24). Using equation (24) and $r_j \in (0, 1)$, a uniformly generated random number between 0 and 1, the index of the selected archive member to serve as a leader is described in equation (25). Consequently, the position and velocity update of *MOPSO* are similar to equations (2) and (3).

$$q_i = \sum_{i=1}^{N} P^i, \quad for\ i = 1\ to\ N \tag{24}$$

$$leader_{index} = find(r_i \leq q_i) \tag{25}$$

G. Mutation Operation in MOPSO

Mutation operator on any j^{th} the selected element is according to equation (26), where ½ is a continuous uniform random number generated between the lower (X_{lb}) and upper (X_{ub}) constraints of the decision variables.

$$Pos_i^{new}(j) = \psi(X_{lb}(j) - X_{ub}(j)) \tag{26}$$

In addition to limitations on decision variables, equation (27) describes X_{lb} and X_{ub}, where $Pos^k(j)$ is the particle's position at the k^{th} iteration and equation (28) defines Δx, which is the additional quantity added or taken due to mutating the particle's position.

$$\begin{cases} X_{(lb)} = \left(Pos^{(k)}(j)\right) - \Delta x \\ X_{(ub)} = \left(Pos^{(k)}(j)\right) + \Delta x \end{cases} \tag{27}$$

$$\Delta x = \xi(X^{\max} - X^{\min}) \tag{28}$$

In equation (28), X^{min} and X^{max} stipulate the minimum and maximum limits of the particle's position $Pos^k(j)$. Equation (29) describes a dynamic mutation scaling factor ✓ [40], where *it* is the current iteration, *Max_it* and mu_r are the maximum iteration and mutation rate, set at 150 and 0.1, respectively.

$$\xi = \left(1 - \frac{it - 1}{Max\_it}\right)^{\left(\frac{1}{mu_r}\right)} \tag{29}$$

Fig. 2 depicts the flowchart of the bi-level approach for coordinated planning of *FACTS-DG*. Fig. 2 comprises parts A, B**,** and C. The inner level consists of parts A and B, while the outer level is mainly part C.

Parts A and B consist of sub-blocks implementing the PI–PSO. In part A, base case ATC is obtained by equation (5). In part B, the algorithm seeks to enhance the base case ATC using PSO to plan TCSC and SSSC optimally, as described in equations (1) to (4). In PI–PSO, a reduced search space is obtained, taking into account the sensitivity of PI concerning the FACTS control parameter. Two approaches were adopted from [2] to reduce masking effects caused by system loading.

Part C is the *MOPSO* according to equations (15) to (29), which depends on the output of *PI–PSO*. Part C also includes a sub-block that plots the Pareto front of *ATC* versus P_{loss} and *ATC* versus V_D, to depict the correlation among objectives.

IV. INTEGRATED TEST NETWORK

Coordination of DN-based DG with an existing transmission-based FACTS requires an *iT&DN*. In Fig. 3, the transmission segment is modeled by the Western System Coordinating Council (WSCC)—buses network and the distribution section by the standard IEEE 16 nodes. Fig. 3a depicts the entire iT&DN in the MATPOWER environment, visualized and validated using STAC—Steady-State AC Network Visualization in the Browser. Fig. 3b describes the simplified one-line diagram showing only the DN section at bus 6 of the WSCC. Similar DN sections are modeled at buses 5, 6, and 8, as shown in Fig. 3a. *iT&DN* comprises nine buses and 48 nodes of transmission and distribution sections, correspondingly numbered successively from 1 to 57. Further details are provided in [9].

V. IMPLEMENTATION ENVIRONMENT

As shown in Fig. 1, the outlined methodology is implemented in the MATLAB/MATPOWER environment [45]. ATC assessment and computations of *PI* sensitivities are executed using MATPOWER while PSO and MOPSO codes are written in MATLAB. While MATLAB runs PSO and MOPSO, MATPOWER computes the objectives by executing the CPF routine for the data exchange. Table I gives the PI–PSO and MOPSO parameters.

VI. RESULTS AND DISCUSSION

Different scenarios of power transfers consisting of bilateral and multilateral transactions are outlined in Table II. The bilateral transactions are *T*1, *T*5, *T*6, *T*8, and *T*9, while the remaining are multilateral transactions. Transfer directions are designated as “Supply Bid” and “Demand Bid.” For comparison of results, after 150 iterations of the MOPSO, a member of the non-dominated solution is considered a reasonable compromise based on two criteria:

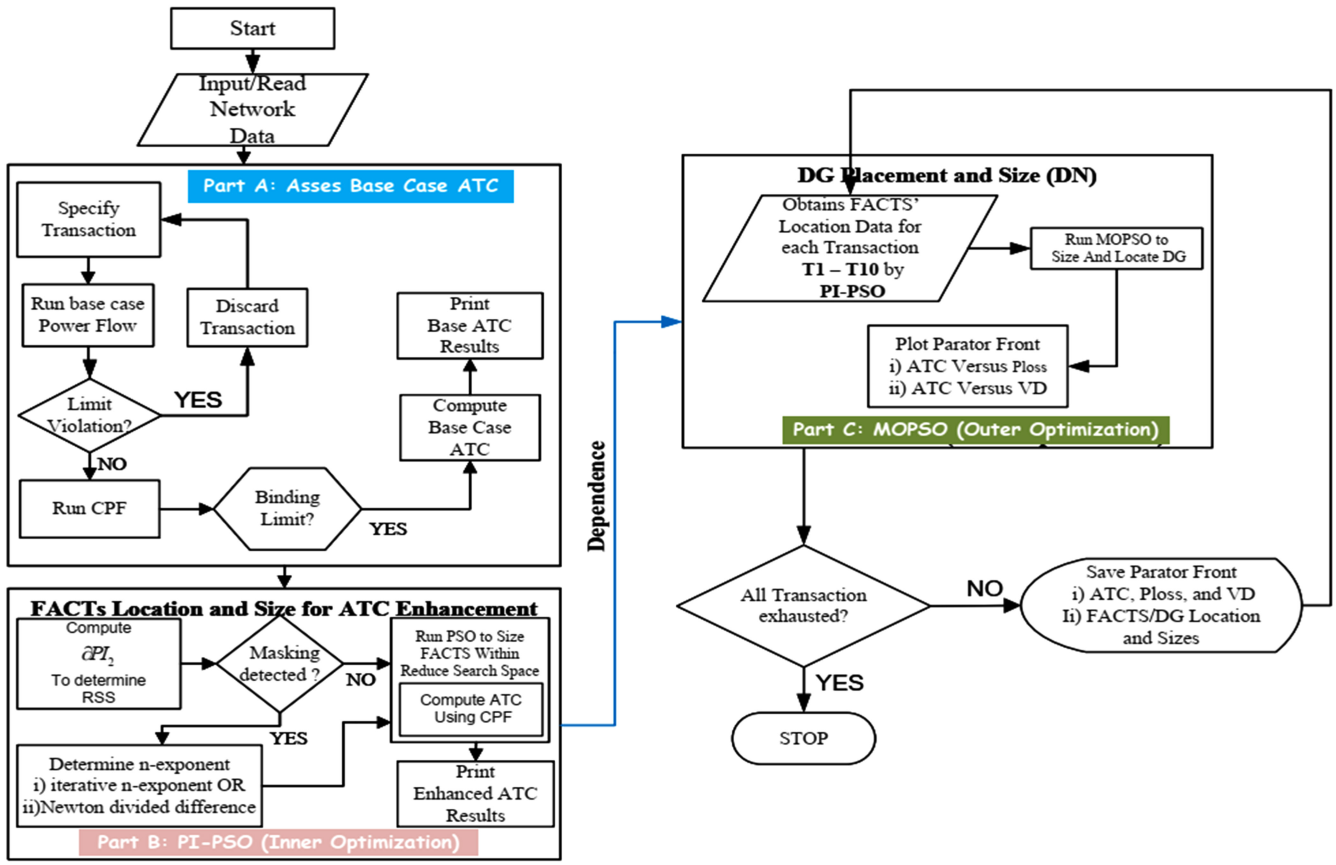

Fig. 2. Flowchart of the bi-level optimization.

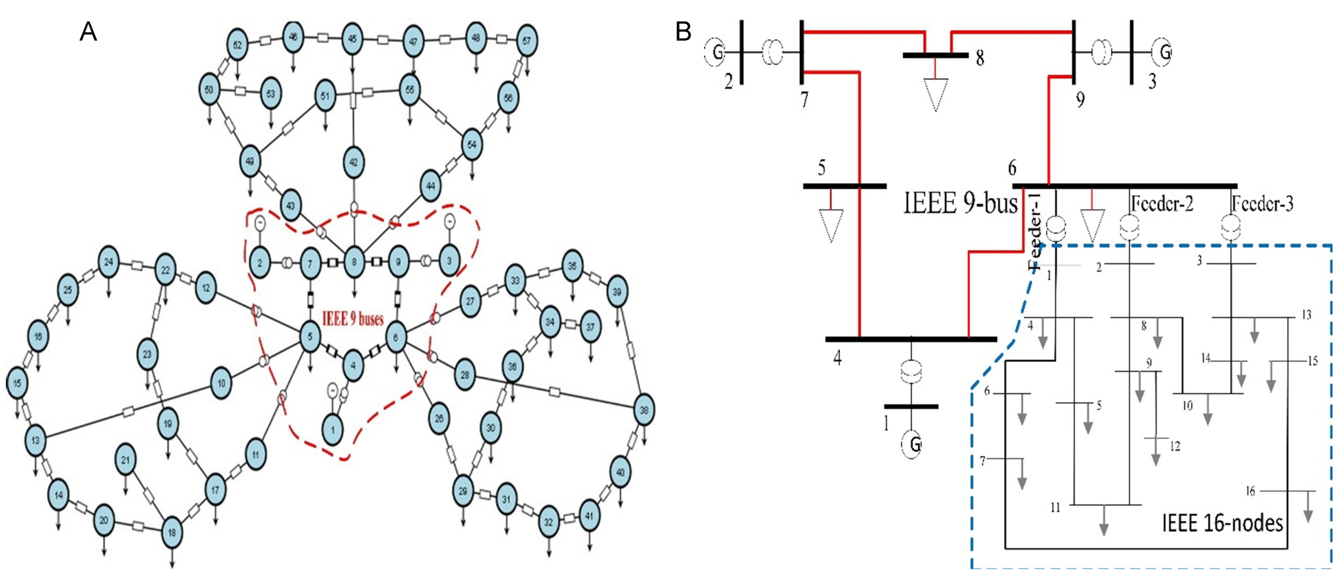

Fig. 3. Integrated test network. (a) Topology in steady-state AC network visualization. (b) A simplified one-line diagram.

TABLE I.
PI–PSO AND MOPSO PARAMETERS

Parameters	PSO	MOPSO	Parameters	PSO	MOPSO	Parameters	PSO	MOPSO
ω_o	0.9	0.5	C_1	1.5	1.0	C_2	$4 - C_1$	2
$\omega damp$	–	0.99	Max_{It}	150	150	$Swarm_{size}$	9	200
ωit	$= 0.1 \times \frac{it-1}{Max\_it-1}$	$= \omega_0 \times 0.99$	Repos.,	–	100	Grids per Dim.	–	7
(α)	–	0.1	β	–	2	γ	–	2
(mu)	–	0.1	–	–	–	–	–	–

MOPSO, multi-objective particle swarm optimization; PSO, particle swarm optimization.

A. Criteria 1

Transfer capability primary criteria described by equation (30) are ATC maximization. Members of archives with superior ATC constitute a solution. In equation (30), $\underset{100}{\mathbf{A}}$ is a vector containing 100 non-dominated solutions, while ATC^0 and ATC^n are ATC before and after coordination, respectively.

$$Pos_i^o \in \underset{100}{\mathrm{A}} \quad if\ ATC^n > ATC^o \tag{30}$$

B. Criteria 2

Dominant objectives: Secondary criteria are based on two dominant objectives as described by equation (31). A solution with two superior objectives is added to $\underset{100}{\mathbf{A}}$. Where $\vec{f}_{i,j}^{0}(x,\lambda)$ and $\vec{f}_{i,j}^{n}(x,\lambda)$ describe the objectives before and after *FACTS-DG* coordination, respectively.

$$Pos_j^o \in \underset{100}{\mathrm{A}} \quad if\ \vec{f}_{i,j}^{n}(x,\lambda) \prec \vec{f}_{i,j}^{o}(x,\lambda) \tag{31}$$

From the list of feasible solutions, one solution is selected based on ATC criteria again. The optimal coordination solutions for *TCSC–DG* and *SSSC–DG* are specified in Table II and III respectively. Since ATC is the primary performance criterion, Fig. 4 compares ATC by TCSC and SSSC with and without DG coordination. From Fig. 4a, TCSC and SSSC significantly enhance the ATC of the above base case. Specifically, TCSC obtains higher ATC in transactions T1 to T5, T8, and T10, while SSSC obtains higher ATC for T6, T7, and T9.

Similarly, Fig. 4b compares ATC between TCSC–PV$_{DG}$ and TCSC–PQ$_{DG}$ while Fig. 4c compares ATC between SSSC–PV$_{DG}$ and SSSC–PQ$_{DG}$. In Fig. 4b and 4c, for all transactions, FACTS and DG coordination

TABLE II.
ENHANCED ATC VALUES FOR TCSC–DG COORDINATION

Trans	Transactions		ATC [MW]			TCSC–PV$_{DG}$ Solution				TCSC–PQ$_{DG}$ Solution			
ID	Supply Bid	Demand Bid	TCSC Only	TCSC-PV$_{DG}$	TCSC-PQ$_{DG}$	P$_{loss}$ [MW]	V$_D$ [p.u.]	TCSC %Comp.	DG$_{Size}$ [MW]	P_{loss} [MW]	V_D [p.u.]	TCSC %Comp.	DG$_{Size}$ [MW, MVar]
T1	1,3	5	154.50	168.83	196.46	6.20	3.82	80	3.96	4.41	3.13	80	[11.24, 13]
T2	1,2	5,8	153.45	153.50	155.31	4.72	3.02	48.91	8.71	4.67	2.44	46.57	[0,13]
T3	1,2,3	5,6	172.11	172.27	174.16	4.82	3.82	80	10.2	4.59	3.31	68.63	[0,12.95]
T4	1,2,3	6,8	178.26	178.89	183.22	4.99	4.16	25.60	21.5	4.86	3.76	41.35	[0,12.99]
T5	2,3	5	64.46	63.59	66.50	2.91	2.32	80	6.38	3.05	2.17	80	[19.76,12.79]
T6	1	8	153.37	168.32	181.92	4.74	2.39	80	21.5	3.62	1.50	80	[21.5,13]
T7	1,2,3	5,8	151.25	151.63	153.74	4.69	3.22	80	11.9	4.69	2.77	52.06	[0.26,12.97]
T8	2,3	6	101.39	101.53	101.98	3.53	3.11	69.12	21.5	3.03	2.65	54.86	[0,13]
T9	1,2	8	79.30	79.63	80.99	2.92	1.98	62.11	14.8	3.12	1.93	46.56	[15.69,13]
T10	1,2	5,6	171.46	169.59	173.97	5.06	4.17	68.35	14.2	4.89	3.82	44.29	[0,10.93]

ATC, available transfer capability; DG, distributed generation; P$_{loss}$, power losses; PQ, reactive power; PV, real power; TCSC, thyristor-controlled series compensator; V$_D$, voltage deviation.

TABLE III.
ENHANCED ATC VALUES FOR SSSC–DG COORDINATION

Trans	ATC [MW]			SSSC–PV_{DG} Solution					SSSC–PQ_{DG} Solution				
ID	SSSC	SSSC	SSSC	P_{loss}	V_D	V_{se}	δ_{se}	DG_{Size}	P_{loss}	V_D	V_{se}	δ_{se}	DG_{Size}
	Only	–PV_{DG}	– PQ_{DG}	[MW]	[p.u.]	[p.u.]	[rad]	[MW]	[MW]	[p.u.]	[p.u.]	[rad]	[MW, MVar]
T1	147.98	155.64	191.21	5.69	4.02	0.07	3.14	3.84	5.77	4.90	0.097	1.40	[5.15,12.86]
T2	152.41	152.63	154.40	4.88	4.08	0.1	2.53	21.5	4.88	3.62	0.1	2.55	[0, 13]
T3	140.9	177.55	195.39	4.24	4.31	0.08	2.06	21.5	4.02	3.83	0.094	2.14	[5.59,13]
T4	177.15	177.54	180.17	5.01	4.36	0.06	1.05	19.8	4.78	3.82	0.066	0.40	[0,13]
T5	63.77	108.59	120.87	2.91	3.55	0.1	1.74	21.5	2.81	3.71	0.099	1.56	[0.25,13]
T6	161.11	180.44	186.20	5.42	3.68	0.09	-0.57	21.5	3.78	2.25	0.097	-0.49	[21.5,13]
T7	152.35	179.18	177.96	4.57	2.46	0.07	2.73	21.5	4.62	2.87	0.046	2.34	[21.5,12.38]
T8	87.58	87.56	98.57	3.01	4.54	0.05	3.05	16.1	3.39	3.78	0.096	1.27	[0,13]
T9	81.44	81.58	82.09	3.50	3.45	0.1	2.69	14.2	3.37	2.71	0.087	2.92	[0,13]
T10	164.78	169.90	173.82	5.15	4.58	0.08	1.12	21.5	4.98	3.52	0.1	0.62	[0,12.76]

PQ, reactive power; PV, real power; SSSC, static synchronous series compensator; TCSC, thyristor-controlled series compensator; VD, voltage deviation.

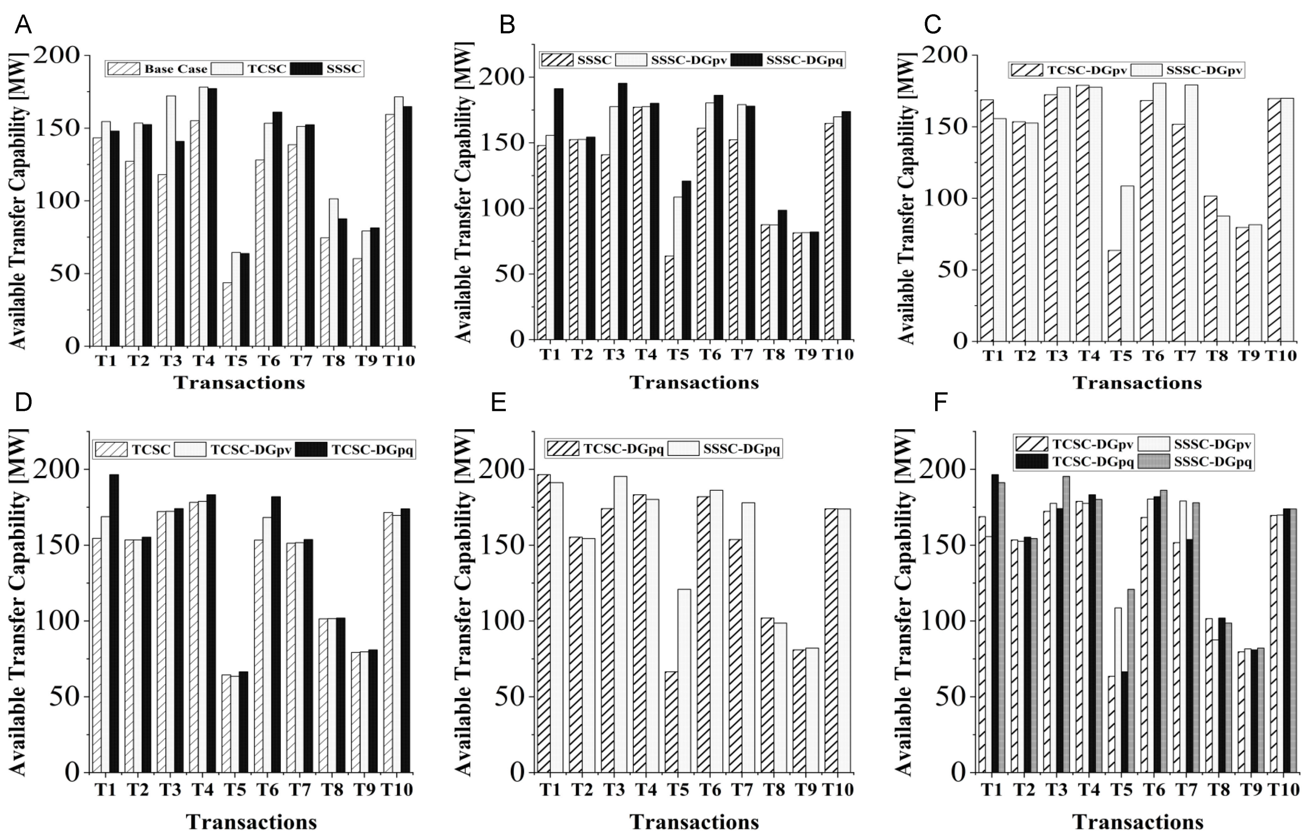

Fig. 4. Performance of FACTS–DG coordination under ATC. (a) TCSC and SSSC. (b) TCSC under PV_{DG} and PQ_{DG}. (c) SSSC under PV_{DG} and PQ_{DG}. (d) TCSC and SSSC under PV_{DG}. (e) TCSC and SSSC under PQ_{DG}. (f) TCSC and SSSC under PV_{DG} and PQ_{DG}. ATC, available transfer capability; FACTS, flexible alternating current transmission systems; DG, distributed generation; PQ, reactive power; PV, real power; SSSC, static synchronous series compensator; TCSC, thyristor-controlled series compensator.

improves the ATC above TCSC or SSSC only. Additionally, coordination with DG models that inject real and reactive power (PQ_{DG}), such as TCSC–PQ_{DG} and SSSC–PQ_{DG} obtains superior ATC. This is attributable to the capability of PQ_{DG} units in supplying reactive power.

Additionally, Fig. 4d compares the ATC under PV_{DG} for TCSC and SSSC, such as TCSC–PV_{DG} and SSSC–PV_{DG}. Furthermore, Fig. 4e compares ATC under PQ_{DG} for TCSC and SSSC, such as TCSC–PQ_{DG} and SSSC–PQ_{DG}. In both Fig. 4d and 4e, observe that the comparison between FACTS under PV_{DG} and PQ_{DG} is said to be transfer-specific. A similar scenario is observed in Fig. 4f, which compares ATC under TCSC–PV_{DG}, SSSC–PV_{DG}, TCSC–PQ_{DG}, and SSSC–PQ_{DG}.

However, the enhanced ATC illustrated in Figs. 4a-f will incur additional power losses, which is the target of DG optimal planning: the reduction of additional power losses incurred at the distribution section due to increased power transfers amounting to enhanced ATC.

Consequently, Fig. 5 depicts a radar plot comparing the performance of TCSC–PV_{DG}, SSSC–PV_{DG}, TCSC–PQ_{DG}, and SSSC–PQ_{DG} in terms of the capability to reduce active power losses. Under T1, with about 42 MW improvements in ATC under TCSC–PQ_{DG} (recorded in Table II), Fig. 5 illustrates a reduced active power loss below the base case. A similar scenario is also observed in transaction T6. In other transactions, although additional power losses above the base case were recorded, the loss distribution for different scenarios was within 1 MW compared to the enhanced ATC recorded.

The optimal planning of FACTS that constitutes the inner optimization level is constrained to the transmission section. Table IV

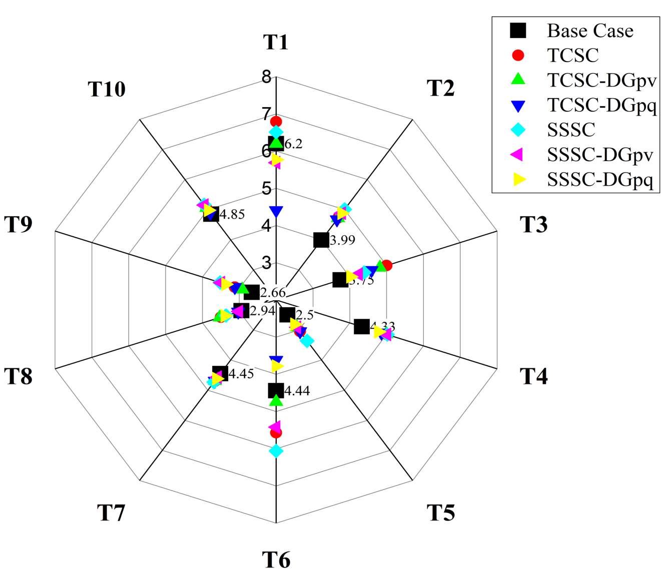

Fig. 5. Performance of FACTS–DG coordination under power losses. FACTS, flexible alternating current transmission systems; DG, distributed generation; SSSC, static synchronous series compensator; TCSC, thyristor-controlled series compensator.

TABLE IV.
OPTIMAL LOCATIONS OF FACTS AND DG IN THE TRANSMISSION AND DISTRIBUTION SECTION

Trans	TCSC Location			SSSC Location		
ID	TCSC	PV_{DG}	PQ_{DG}	SSSC	PV_{DG}	PQ_{DG}
T1	8 (9 to 6)	21	18	6 (8 to 9)	21	18
T2	3 (5 to 7)	10	56	5 (7 to 8)	29	19
T3	8 (9 to 6)	49	18	3 (5 to 7)	10	13
T4	3 (5 to 7)	28	45	8 (9 to 6)	27	45
T5	8 (9 to 6)	31	11	3 (5 to 7)	10	17
T6	9 (6 to 4)	50	50	5 (7 to 8)	50	50
T7	5 (7 to 8)	42	56	6 (8 to 9)	42	43
T8	8 (9 to 6)	48	34	2 (4 to 5)	18	36
T9	3 (5 to 7)	36	44	5 (7 to 8)	43	47
T10	5 (7 to 8)	26	14	2 (4 to 5)	28	37

PQ, reactive power; PV, real power; SSSC, static synchronous series compensator; TCSC, thyristor-controlled series compensator.

gives the optimal locations of FACTS in coordination with either PV_{DG} or PQ_{DG}. From Tables II and IV, superior ATC for T1 is achieved with TCSC optimally placed on line 8 (9 to 6) at 80% compensation, in coordination with PQ_{DG} optimally placed at node 18, having real and reactive power injections of 11.24 MW and 13 MVAr, respectively. It is noted that the optimal location is specific to the power transfer direction. Although the optimal location of TCSC for multiple transactions such as T1, T3, T5, and T8 is the same, the percentage of TCSC compensation differs depending on the transactions and model of DG. For example, TCSC–PV_{DG} Under T4, an ATC of 178.3 MW was obtained with a power loss of 4.99 MW at 25.60 % TCSC compensation. While for the same T4, with TCSC–PQ_{DG} the ATC improves to 183.22 MW with 4.86 MW power loss at 41.35% TCSC compensation. The increased TCSC compensation has associated cost implications. The reduced power loss is due to increased TCSC compensation and the capability of PQ_{DG} to supply reactive power.

Similarly, from Tables III and IV, the superior ATC for T3 is with SSSC optimally placed at line 3 (5 to 7), with series voltage injection V_{se} of 0.094 p.u. $\angle$ 2.14 rad, while DG optimally placed at node 13 has real and reactive power injections of 5.59 MW and 13 MVAr, respectively. Generally, from Tables III and IV, the TCSC–PQ_{DG} and SSSC–PQ_{DG} obtains improved ATC compared to TCSC–DG_{PV} and SSSC–DG_{PV} for all transactions.

Numerical comparison of ATC values with TCSC only, SSSC only, and FACTS–DG coordination using the hybrid PI-PSO and MOPSO, respectively, is given in Fig 4. Furthermore, Figs. 6, 7, and 8 illustrates the convergence characteristics for a typical run of PSO and PI–PSO with TCSC and SSSC. Although ATC by PI–PSO is slightly higher in some transactions, PSO produces similar ATC under TCSC, which is attributable to

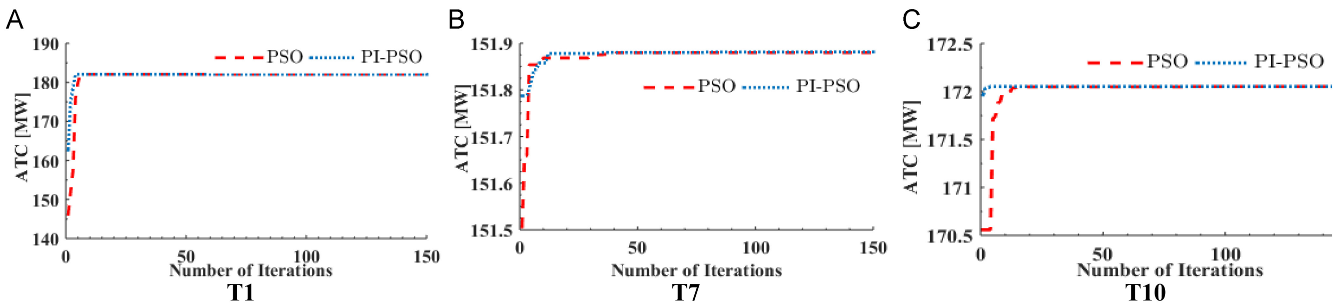

Fig. 6. Convergence curve of PI–PSO and PSO for ATC enhancement with TCSC. ATC, available transfer capability; PI, performance index; PSO, particle swarm optimization.

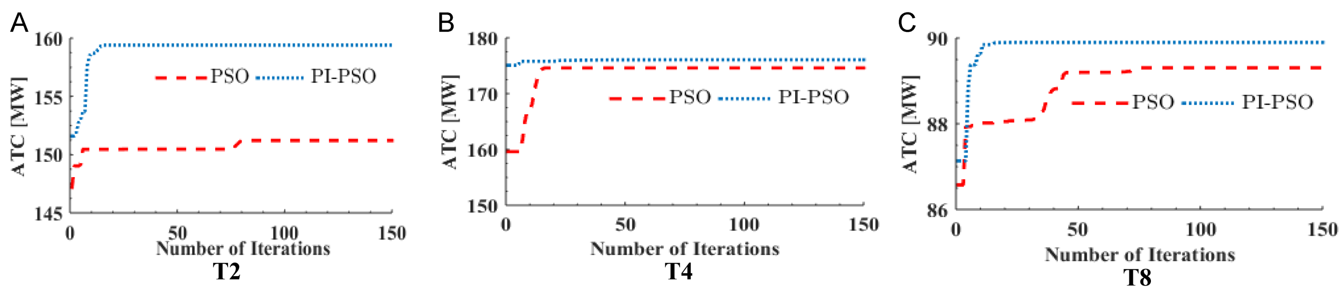

Fig. 7. Convergence curve of PI–PSO and PSO for ATC enhancement with SSSC. ATC, available transfer capability; PI, performance index; PSO, particle swarm optimization.

the non-complex nature of TCSC's control parameter. Observe that due to the reduced search space in PI–PSO, there was improvement in the random starting point of PI–PSO compared to PSO. The improved performance of PI–PSO over PSO can be attributable to better exploration capabilities of PI–PSO. This improves the random particle's position starting point within the reduced search space as depicted in Fig. 8, which compares the plots of particles' positions against FACTS controllable parameter using PSO and PI–PSO with SSSC.

After 150 iterations, the non-dominated solution establishes a correlation among objectives through 3D plots. For some selected transactions T1 to T3, the 3D Pareto front plots are depicted in Figs. 9 and 10 for TCSC and SSSC, respectively.

The non-dominated 3D Pareto front plots are depicted in Figs. 9a-c and Figs. 10a-c for TCSC and SSSC separately. It is observed that the 3D Pareto plots show a diving parabola. The correlation helps system operators share resources to meet market demands in a coordinated manner. The transmission system operator can approximate the transfer limit in coordination with the distribution system operator's resources.

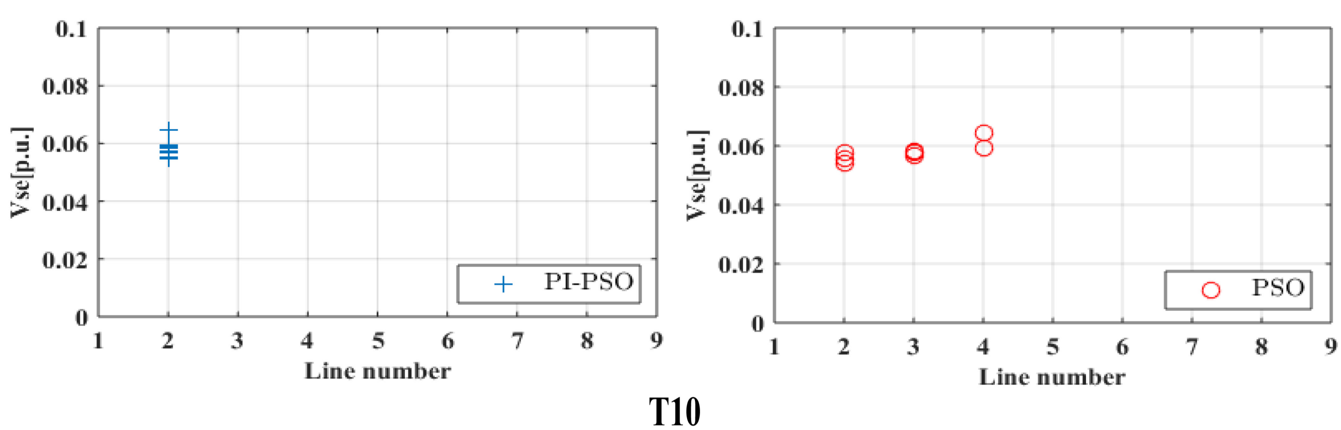

Fig. 8. A typical plot of particles' positions versus V_{se} for PI–PSO and PSO with SSSC. PI, performance index; PSO, particle swarm optimization; SSSC, static synchronous series compensator.

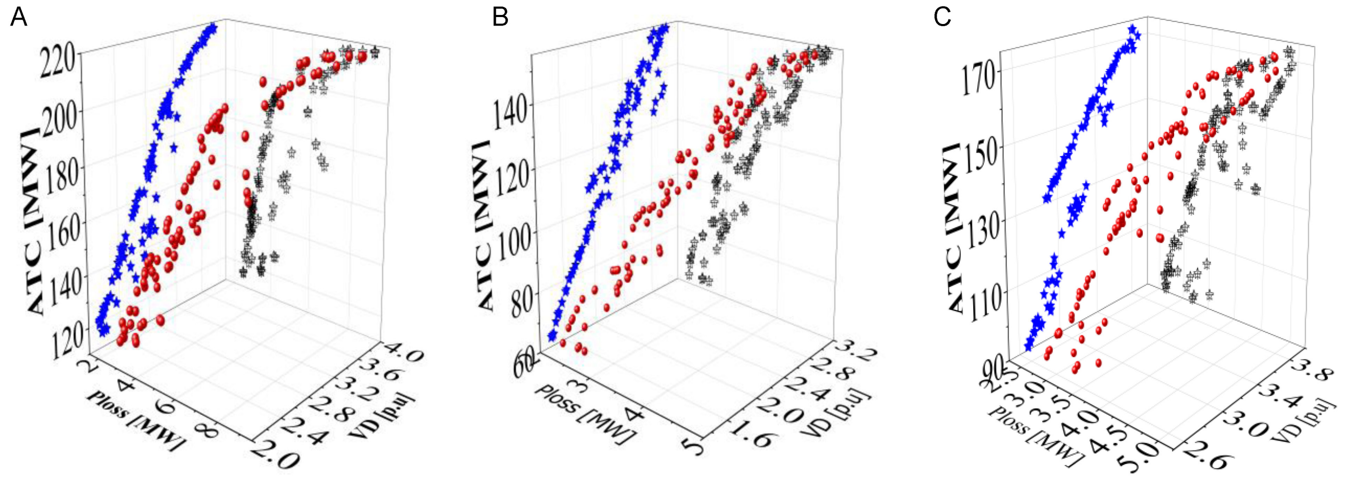

Fig. 9. Pareto front plot for different transactions under TCSC–DG coordination. (a) T1 TCSC–PQ_{DG}, (b) T2 TCSC–PV_{DG}, (c) T3 TCSC–PV_{DG} ATC, available transfer capability; PQ, reactive power; PV, real power; TCSC, thyristor-controlled series compensator.

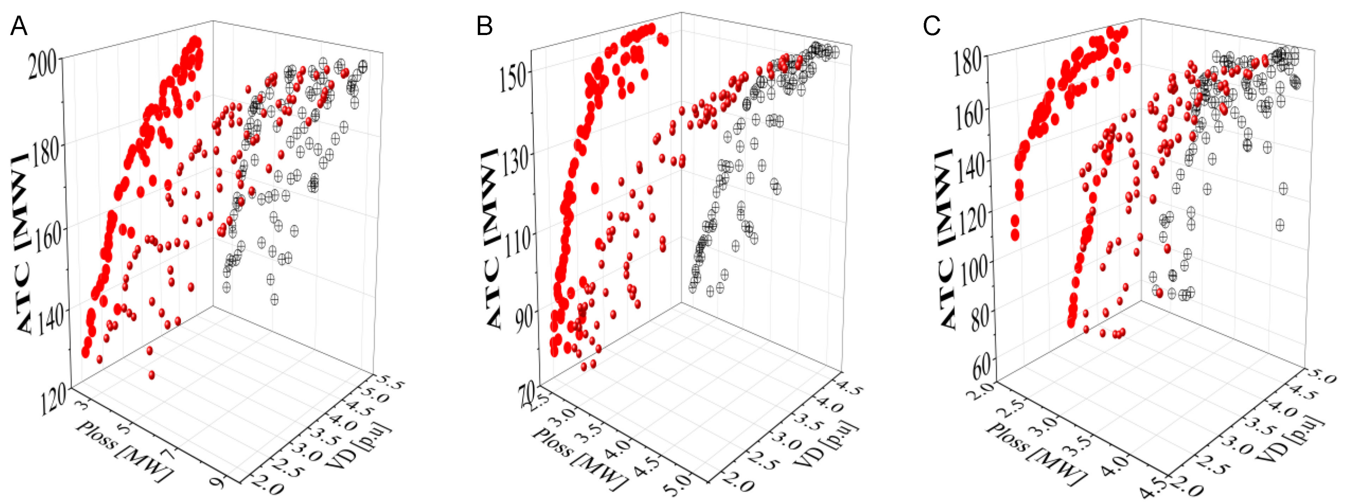

Fig. 10. Pareto front plot for different transactions under SSSC–DG Coordination. (a) T1 SSSC–PQ_{DG}, (b) T2 SSSC–PV_{DG}, (c) T3 SSSC–$V_{DG.}$

From the 3D Pareto front plots, further insight can be obtained in terms of the correlation between any two objectives, such as ATC versus P_{loss}, ATC versus V_D, and P_{loss} versus V_D. Consequently, the Pareto plot slices of ATC versus P_{loss} and ATC versus V_D are obtained and shown in Figs. 11 and 12 for TCSC and SSSC, respectively. The slices also depict convergence characteristics of the non-dominated solution, which guides the system operator's decision in accepting power supply bids.

For T1, under the TCSC–PQ_{DG} coordination, it is observed from Figs. 11a and 11b, and Table II, an improved ATC with *TCSC* from

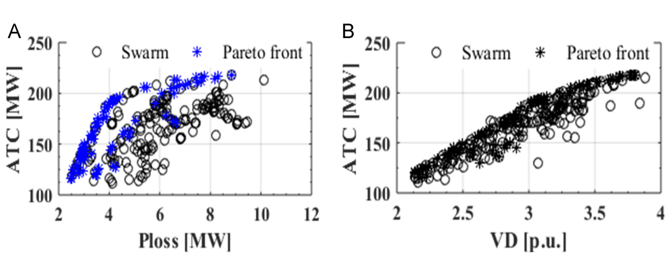

Fig. 11. Slices of Pareto plot for transaction T1 under TCSC–PQ_{DG}. (a) ATC versus power loss (P_{loss}) (b) ATC versus voltage deviation (V_D).

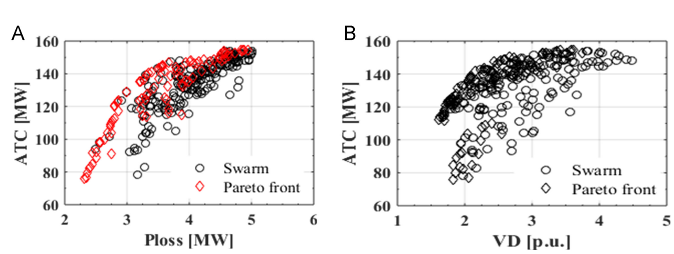

Fig. 12. Slices of Pareto plot for transaction T2 under SSSC–PQ_{DG}. (a) ATC versus power loss (P_{loss}) (b) ATC versus voltage deviation (V_D).

154.50 MW without DG coordination to 200 MW with PQ_{DG}. The improvement in ATC is at a reduced P_{loss} and V_D of 4.5 MW and 3.2 p.u, respectively. Furthermore, the slope of the Pareto front in Fig. 11b is approximately constant. At the same time, the parabolic-like shape of Fig. 11a depicts a non-linear slope approaching zero after a maximum ATC above 200 MW. The point of zero slope implies an increasing P_{loss} with approximately constant ATC. Further power transfer above this point is not economical. Similarly, for T2, Figs. 12a and 12b depict a non-linear slope approaching zero above an ATC of 155 MW.

VII. CONCLUSION

This paper develops a bi-level approach to FACTS and DG coordination in an *iT & DN*. TCSC and SSSC were separately coordinated with PV and PQ types of DG. The coordination involves multiple objectives at the transmission and distribution sections. It is concluded that the coordinated planning of transmission and DN resources enhances competitive market operations through improved ATC, reduced P_{loss}, and the maintenance of quality voltage profiles. It was observed that the TCSC-PQ_{DG} and SSSC-PQ_{DG} obtain enhanced ATC values with the best compromise in reducing active P_{loss} and V_{D}. Also, from the 3D and 2D plots of the Pareto front for various transactions, there exists some maximum ATC, above which the slope of the Pareto approaches zero. The zero slope indicates that after the maximum ATC point, an attempt to further to improve the ATC with FACTS at such a location incurs additional P_{loss} without an equivalent enhancement in the ATC. Henceforth, this information will aid operators in decision-making, especially in a competitive market. Furthermore, it is noted that depending on the system loading represented by transfer direction, the correlation between ATC against P_{loss} and ATC against V_{D} depicts a diving parabolic-like shape.

Peer-review: Externally peer-reviewed.

Author Contributions: Concept – A.A.S.; Design – A.A.S., L.Y., M.B., S.S.A.; Supervision – S.S.A., M.B.; Funding – A.A.S.; Materials – A.A.S., L.Y.; Data Collection and/or Processing A.A.S., L.Y.; Analysis and/or Interpretation – M.B., A.A.S., S.S.A.; Literature Review – A.A.S., M.B., L.Y.; Writing – A.A.S., J.G.A.; Critical Review – J.G.A., S.S.A.

Declaration of Interests: The authors declare that they have no competing interests.

Funding: This study received no funding.

REFERENCES

1. S. D. Patil, R. A. Kachare, A. M. Mulla, and D. R. Patil, "Performance enhancement of modified SVC as a thyristor binary switched capacitor and reactor banks by using different adaptive controllers," *J. King Saud Univ. Eng. Sci.*, vol. 35, no. 5, 342–357, 2023. [CrossRef]
2. A. A. Sadiq, S. S. Adamu, and M. Buhari, "Available transfer capability enhancement with FACTS using hybrid PI-PSO," *Turk J. Elec Eng & Comp Sci*, vol. 27, no. 4, pp. 2881–2897, 2019. [CrossRef]
3. X. Zhang, K. Tomsovic, and A. Dimitrovski, "Optimal allocation of series FACTS devices in large-scale systems," *IET Gener. Transm. Distrib.*, vol. 12, no. 8, pp. 1889–1896, 2018. [CrossRef]
4. P. C. Sahu, R. C. Prusty, and S. Panda, "Approaching hybridized GWO-SCA based type-II fuzzy controller in AGC of diverse energy source multi-area power system," *J. King Saud Univ. Eng. Sci.*, vol. 32, no. 3, pp. 186–197, 2020. [CrossRef]
5. M. S. Rawat, and S. Vadhera, "A novel method for determination of maximum penetration of distributed generation in radial distribution network," *Aust. J. Electr. Electron. Eng.*, vol. 18, no. 2, pp. 80–90, 2021. [CrossRef]
6. K. S. Sambaiah, "Optimal Distributed Generation Allocation in Practical Distribution System in the Presence of Plug-in Electric Vehicles", *TEPES*, vol. 3, no. 1, pp. 2–11, 2023. [CrossRef]
7. U. Sur, "Impact study of distributed generations in voltage sag mitigation using an improved three-phase unbalanced load flow for active distribution network,", *TEPES*, vol. 2, no. 2, pp. 124–133, 2022. [CrossRef]
8. J. M. Bloemink, and T. C. Green, "Benefits of distribution-level power electronics for supporting distributed generation growth," *IEEE Trans. Power Deliv.*, vol. 28, no. 2, pp. 911–919, 2013. [CrossRef]
9. A. A. Sadiq, S. S. Adamu, and M. Buhari, "Optimal distributed generation planning in distribution networks: A comparison of transmission network models with FACTS," *Eng. Sci. Technol. An Int. J.*, vol. 22, no. 1, pp. 33–46, 2019. [CrossRef]
10. P. K. Pandey, and B. Bag, "A comparative study on UPFC and SVC towards voltage profile improvement of a grid-connected distributed generation system," in 2015 International Conference on Energy, Power and Environment: Towards Sustainable Growth, ICEPE, 2015, 2015, pp. 1–5. [CrossRef]
11. Y. Feng, S. Wang, C. Xue, Y. Cao, J. Wu, and H. Li, "Flexible coordinated optimal operation model of 'source-grid-load-storage' in smart distribution network," in Proceedings - 2020 5th Asia Conference on Power and Electrical Engineering, ACPEE 2020, Vol. 2020, 2020, pp. 2231–2236. [CrossRef]
12. K. Fatima, M. Sefid, M. A. Anees, and M. Rihan, "An investigation of the impact of synchrophasors measurement on multi-area state estimation in active distribution grids," *Aust. J. Electr. Electron. Eng.*, vol. 17, no. 2, pp. 122–131, 2020. [CrossRef]
13. J. Fang, H. Wang, F. Yang, K. Yin, X. Lin, and M. Zhang, "A failure prediction method of a power distribution network based on PSO and XGBoost," *Aust. J. Electr. Electron. Eng.*, pp. 1–8, 2022. [CrossRef]
14. H. Gerard, E. I. Rivero Puente, and D. Six, "Coordination between transmission and distribution system operators in the electricity sector: A conceptual framework," *Util. Policy*, vol. 50, pp. 40–48, 2018. [CrossRef]
15. E. Boutsiadis, D. Tsiamitros, and D. Stimoniaris, "Ripple Signaling Control for Ancillary Services in Distribution Networks," *TEPES*, vol. 2, no. 1, pp. 31–45, 2022. [CrossRef]
16. A. G. Givisiez, K. Petrou, and L. F. Ochoa, "A review on TSO-DSO coordination models and solution techniques," *Electr. Power Syst. Res.*, vol. 189, pp. 106659, 2020. [CrossRef]
17. E. Doğan, and N. Yörükeren, "Enhancement of Transmission System Security with Archimedes Optimization Algorithm," *TEPES*, vol. 2, no. 2, pp. 115–123, 2022. [CrossRef]
18. H. Jain, K. Rahimi, A. Tbaileh, R. P. Broadwater, A. K. Jain, and M. Dilek, "Integrated transmission and distribution system modeling and analysis: Need and advantages," *IEEE Power Energy Soc. Gen. Meet. (PESGM)*, vol. 2016, pp. 1–5, 2016. [CrossRef]
19. S. Li, T. Yu, T. Pu, J. Ming, and S. Fan, "Coordinated optimization control method of transmission and distribution network," in Asia-Pacific Power and Energy Engineering Conference, APPEEC, 2016, pp. 2215–2219. [CrossRef]
20. G. Mu, J. Contreras, J. M. Arroyo, A. Sanchez de la Nieta, and M. Gibescu, "Integrated transmission and distribution system expansion planning under uncertainty," *IEEE Trans. Smart Grid*, vol. 12, no. 5, pp. 4113–4125, 2021. [CrossRef]
21. M. Nadeem *et al.*, "Optimal placement, sizing and coordination of FACTS devices in transmission network using whale optimization algorithm," *Energies*, vol. 13, no. 3, pp. 1–24, 2020. [CrossRef]

22. A. A. Sadiq, S. Sani Adamu, and M. Buhari, "Multi-type FACTS location and coordination using PI-PSO for transfer capability improvement," in IEEE PES/IAS PowerAfrica Conference: Power Economics and Energy Innovation in Africa, Power Africa, vol. 2019, pp. 662–667, 2019. [CrossRef]
23. A. A. Sadiq, M. Buhari, S. S. Adamu, and H. Musa, "Coordination of multi-type FACTS for available transfer capability enhancement using PI-PSO," *IET Gener. Transm. Distrib.*, vol. 14, no. 21, pp. 4866–4877, 2020. [CrossRef]
24. S. R. Ghatak, S. Sannigrahi, and P. Acharjee, "Optimised planning of power distribution network with solar energy, Battery storage and DSTATCOM: A multi-objective approach," in 2018 IEEE International Conference on Power Electronics, Drives and Energy Systems (PEDES), Vol. 2018, 2018, pp. 1–6. [CrossRef]
25. H. Saberi, S. Mehraeen, and B. Wang, "Stability improvement of microgrids using a novel reduced UPFC structure via non-linear optimal control," in 2018 IEEE Applied Power Electronics Conference and Exposition (APEC), Vol. 2018, 2018, pp. 3294–3300. [CrossRef]
26. T. F. Orchi, M. J. Hossain, H. R. Pota, and M. S. Rahman, "Impact of distributed generation and series compensation on distribution network," in Proceedings of the 2013 IEEE 8th Conference on Industrial Electronics and Applications, ICIEA, Vol. 2013, 2013, pp. 854–859. [CrossRef]
27. Ravi, and R. Raman, "Coordination between SVC and OLTC for voltage control in Wind Energy Conversion System," *International Research Journal of Engineering and Technology (IRJET)*, vol. 3, no. 10, pp. 482–485, 2016. [CrossRef]
28. J. Shi, A. Kalam, and P. Shi, "Improving power quality and stability of wind energy conversion system with fuzzy-controlled STATCOM," *Aust. J. Electr. Electron. Eng.*, vol. 12, no. 3, pp. 183–193, 2015. [CrossRef]
29. E. Basak, and B. A. Aysen, "Power Quality Evaluation of Distributed Generation Systems,". *TEPES*, vol. 1, no. 1, pp. 12–18, 2021. [CrossRef]
30. D. Shukla, S. P. Singh, and S. R. Mohanty, "Optimal Strategy for ATC Enhancement and Assessment in the presence of FACTS devices and Renewable Generation," in Proceedings of the National Power Systems Conference (NPSC), 2018, pp. 12–17. [CrossRef]
31. B. Mahdad, and K. Srairi, "Adaptive Differential Search Algorithm for Optimal Location of Distributed Generation in the presence of SVC for Power Loss Reduction in Distribution System," *Eng. Sci. Technol. An Int. J.*, vol. 19, no. 3, pp. 1266–1282, 2016. [CrossRef]
32. M. S. Rahman, M. A. Mahmud, A. M. T. Oo, H. R. Pota, and M. J. Hossain, "Agent-based reactive power management of power distribution networks with distributed energy generation" *Energy Convers. Manag.*, vol. 120, pp. 120–134, 2016. [CrossRef]
33. H. B. Tolabi, M. H. Ali, and M. Rizwan, "Simultaneous Reconfiguration, Optimal Placement of DSTATCOM, and Photovoltaic Array in a Distribution System based on Fuzzy-ACO Approach," *IEEE Trans. Sustain. Energy*, vol. 6, no. 1, pp. 210–218, 2015. [CrossRef]
34. M. Farsadi, F. M. Shahir, D. Nazarpour, and F. N. Heris, "Analyzing of coordinate operational of UPFC based on matrix converter and wind turbine generator under unbalanced load," in ELECO 2015 - 9th International Conference on Electrical and Electronics Engineering, vol. 2016, pp. 525–529, 2015. [CrossRef]
35. B. Singh, V. Mukherjee, and P. Tiwari, "GA-based optimization for optimally placed and properly coordinated control of distributed generations and Static Var Compensator in distribution networks," *Energy Rep.*, vol. 5, pp. 926–959, 2019. [CrossRef].
36. F. Ugranli, and E. Karatepe, "Coordinated TCSC allocation and network reinforcements planning with wind power," *IEEE Trans. Sustain. Energy*, vol. 8, no. 4, pp. 1694–1705, 2017. [CrossRef]
37. A. Mirzapour-Kamanaj, M. Majidi, K. Zare, and R. Kazemzadeh, "Optimal strategic coordination of distribution networks and interconnected energy hubs: A linear multi-follower bi-level optimization model," *Int. J. Electr. Power Energy Syst.*, vol. 119, pp. 1–12, 2020. [CrossRef]
38. E. S. Ali, S. M. Abd-Elazim, and A. Y. Abdelaziz, "Ant lion optimization algorithm for renewable distributed generations," *Energy*, vol. 116, pp. 445–458, 2016. [CrossRef]
39. S. A. Chithradevi, L. Lakshminarasimman, and R. Balamurugan, "Stud krill herd algorithm for multiple DG placement and sizing in a radial distribution system," *Eng. Sci. Technol. An Int. J.*, vol. 20, no. 2, pp. 748–759, 2017. [CrossRef]
40. A. Britto, and A. Pozo, "I-MOPSO: A suitable PSO algorithm for many-objective optimization," in Proceedings - Brazilian Symposium on Neural Networks, 2012, pp. 166–171. [CrossRef]
41. P. K. Tripathi, S. Bandyopadhyay, and S. K. Pal, "Multi-objective particle swarm optimization with time-variant inertia and acceleration coefficients," *Inf. Sci. (Ny).*, vol. 177, no. 22, pp. 5033–5049, 2007. [CrossRef]
42. H. Farahmand, M. Rashidinejad, A. Mousavi, A. A. Gharaveisi, M. R. Irving, and G. A. Taylor, "Hybrid mutation particle swarm optimisation method for available transfer capability enhancement," *Int. J. Electr. Power Energy Syst.*, vol. 42, no. 1, pp. 240–249, 2012. [CrossRef]
43. E. S. Ali, S. M. A. Elazim, and A. Y. Abdelaziz, "Ant lion optimization algorithm for optimal location and sizing of renewable distributed generations," *Renew. Energy*, vol. 101, pp. 1311–1324, 2017. [CrossRef]
44. A. A. Sadiq, M. Buhari, J. G. Ambafi, S. S. Adamu, and M. N. Nwohu, "Contingency constrained TCSC and DG coordination in an integrated transmission and distribution network: A multi-objective approach," *e-Prime - Adv. Electr. Eng. Electron Energy*, vol. 4, pp. 100156, 2023. [CrossRef]
45. R. D. Zimmerman, C. E. Murillo-Sanchez, and R. J. Thomas, "MATPOWER: Steady-state operations, planning, and analysis tools for Power Systems Research and education," *IEEE Trans. Power Syst.*, vol. 26, no. 1, pp. 12–19, 2011. [CrossRef]